HAL
open science

Enhanced electron heating in the magnetic nozzle of a radio-frequency plasma via electron cyclotron resonance

Alfio Vinci, Stéphane Mazouffre

To cite this version:

Alfio Vinci, Stéphane Mazouffre. Enhanced electron heating in the magnetic nozzle of a radio-frequency plasma via electron cyclotron resonance. EPL - Europhysics Letters, 2023, 141 (4), pp.44002. 10.1209/0295-5075/acb967 . hal-04020712

HAL Id: hal-04020712

https://hal.science/hal-04020712v1

Submitted on 9 Mar 2023

HAL is a multi-disciplinary open access archive for the deposit and dissemination of scientific research documents, whether they are published or not. The documents may come from teaching and research institutions in France or abroad, or from public or private research centers.

L'archive ouverte pluridisciplinaire **HAL**, est destinée au dépôt et à la diffusion de documents scientifiques de niveau recherche, publiés ou non, émanant des établissements d'enseignement et de recherche français ou étrangers, des laboratoires publics ou privés.

A LETTERS JOURNAL EXPLORING THE FRONTIERS OF PHYSICS

ACCEPTED MANUSCRIPT

Enhanced electron heating in the magnetic nozzle of a radio-frequency plasma via electron cyclotron resonance

To cite this article before publication: Alfio Emanuele Vinci *et al* 2023 *EPL* in press https://doi.org/10.1209/0295-5075/acb967

Manuscript version: Accepted Manuscript

Accepted Manuscript is "the version of the article accepted for publication including all changes made as a result of the peer review process, and which may also include the addition to the article by IOP Publishing of a header, an article ID, a cover sheet and/or an 'Accepted Manuscript' watermark, but excluding any other editing, typesetting or other changes made by IOP Publishing and/or its licensors"

This Accepted Manuscript is **Copyright © EPLA, 2023**.

During the embargo period (the 12 month period from the publication of the Version of Record of this article), the Accepted Manuscript is fully protected by copyright and cannot be reused or reposted elsewhere.
As the Version of Record of this article is going to be / has been published on a subscription basis, this Accepted Manuscript is available for reuse under a CC BY-NC-ND 3.0 licence after the 12 month embargo period.

After the embargo period, everyone is permitted to use copy and redistribute this article for non-commercial purposes only, provided that they adhere to all the terms of the licence https://creativecommons.org/licences/by-nc-nd/3.0

Although reasonable endeavours have been taken to obtain all necessary permissions from third parties to include their copyrighted content within this article, their full citation and copyright line may not be present in this Accepted Manuscript version. Before using any content from this article, please refer to the Version of Record on IOPscience once published for full citation and copyright details, as permissions will likely be required. All third party content is fully copyright protected, unless specifically stated otherwise in the figure caption in the Version of Record.

View the article online for updates and enhancements.

This content was downloaded from IP address 91.166.247.18 on 07/02/2023 at 06:48

Enhanced electron heating in the magnetic nozzle of a radio-frequency plasma via electron cyclotron resonance

Alfio E. Vinci[1] [(a)] and Stéphane Mazouffre[1] [(b)]

[1] *Institut de Combustion, Aérothermique, Réactivité et Environnement, Centre National de la Recherche Scientifique, 1C Avenue de la Recherche Scientifique, 45071 Orléans, France*

Abstract – The effect of electron cyclotron resonance on the electron flow is experimentally examined in the magnetic nozzle of a radio-frequency plasma source powered at 13.56 MHz under a series of operating conditions. Measurements of the electron energy probability function show that the bulk of electrons is effectively heated when the external magnetic field meets the cyclotron resonance condition in the proximity of the antenna. A careful tuning of the magnetic field topology inside the plasma source leads to a gain in electron density and temperature up to about 20 % and 40 %, respectively.

Introduction. – Efficient plasma generation and acceleration are essential aspects in the field of electric propulsion (EP). Research on physics and technology continuously addresses these challenges to advance novel EP concepts having certain enabling characteristics, e.g. longer lifetime and compatibility with non-conventional propellants like iodine and water [1–3]. These qualities support the interest in electrodeless devices based on either radio-frequency (rf) [4–7] or microwave discharges [8]. Such plasma sources rely on an external magnetic field to meet the conditions for efficient collisionless heating via interaction with the electromagnetic fields. Typically, the applied magnetic field also shapes a magnetic nozzle (MN) that extends downstream the discharge chamber. The MN is the main driver for plasma acceleration and electromagnetic thrust production. In typical electrodeless discharges, e.g. helicon plasma thrusters (HPT) and electron-cyclotron resonance thrusters (ECRT), input power couples to the electron population in the form of thermal energy, which is spent for ionization and ion acceleration. The latter occurs through ambipolar electric field [9] and diamagnetic electron drift [10], eventually leading to supersonic ion velocities in the MN. In order to maximize the momentum gained by the ions, efforts should focus on: *i*) reducing the fraction of neutrals in the plume which represent a drag contribution via collisions [11, 12]; *ii*) maximizing the thermal energy at the MN inlet available for conversion into ion kinetic energy. Accordingly, the key parameter that inherently rules the MN phenomena is the electron temperature T_e. Values of T_e up to tens of eV have been recorded in ECRTs [13, 14] at very low input power, whereas in rf discharges it seldom exceeds 10 eV. As a matter of fact, microwave devices can provide larger thrust efficiency at much lower power levels with respect to rf-based thrusters, whose competitiveness instead manifests in the kW range [7]. However, implementation of electrodeless ECR systems on-board of small spacecrafts might not be trivial, given the state-of-the-art of microwave power units [15–21]. This could be particularly true whenever the required input power exceeds tens of W and the system size is reduced, which translates into operating frequencies above 5 GHz [8]. Theoretically, though, it is possible to combine rf power and electron-cyclotron resonance in one single device without resorting to microwave sources, provided that the external magnetic field meets the ECR condition while the discharge stability is not compromised. At the typical rf operating frequency, i.e. 13.56 MHz, a magnetic field intensity equal to $B_{res} = \omega_{ce} m_e / e \simeq 0.484$ mT satisfies the resonance condition. This approach has been previously studied for plasma processing applications in an inductive discharge [22, 23] reporting effective heating of low energy electrons due to anomalous skin effect. Thus far, a similar approach applied to MN for propulsion purposes remains completely unexplored.

Experimental setup. – This study investigates how electrons in a MN are influenced when the ECR condition

(a) E-mail: alfio.vinci@cnrs-orleans.fr
(b) E-mail: stephane.mazouffre@cnrs-orleans.fr

Accepted Manuscript

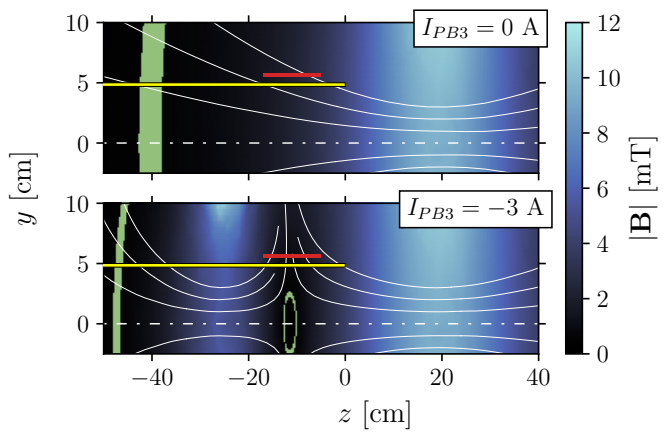

Fig. 1: 2-D maps of the external magnetic field. The yellow rectangle depicts the source tube, whereas the red line identifies the antenna location. Magnetic streamlines are shown as white solid lines. The green pixels highlight the location where $|\mathbf{B}|$ equals the resonance value ($\pm 10\,\%$).

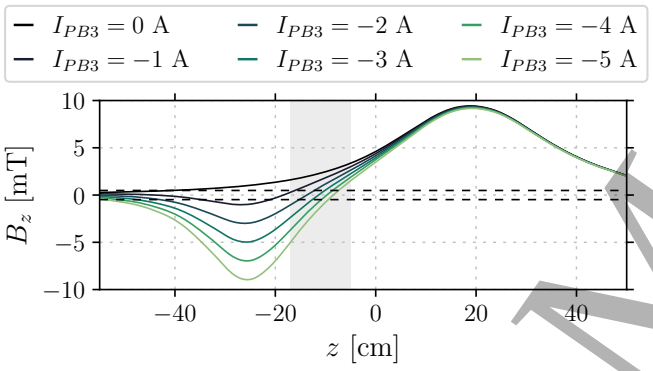

Fig. 2: On-axis z-component of the external magnetic field for different values of I_{PB3}. The current flowing in GB2 is fixed to 9 A. The gray shaded area indicates the antenna region, while the black dashed lines identify the resonance value of the magnetic field strength.

is met near the rf antenna. Measurements are performed in a helicon-like plasma source, whose main characteristics have been reported in [5,6,24]. The tube constituting the discharge chamber is made in borosilicate glass with $\phi = 9.4$ cm inner diameter and $L = 55$ cm length. The origin of the axial coordinate z is defined to coincide with the tube open boundary. The latter is connected to a 30 cm in inner diameter and 50 cm in length expansion chamber. The ultimate base pressure is around 8×10^{-6} mbar, whereas the typical pressure during operation reads about 3×10^{-3} mbar. Xenon, currently the preferred propellant for electric thrusters [25, 26], is introduced axially at the back plate of the tube through a multi-perforated grid. The rf antenna in use here is a double-saddle type with 12 cm length centered at $z \simeq -11$ cm. It is fully made of copper and it is directly connected to a custom π-type matching network. Input power is generated by a 1 kW-class commercial power supply at 13.56 MHz. Matching of the rf power is manually attained and the reflected power is always below $1 - 2$ % during operation.

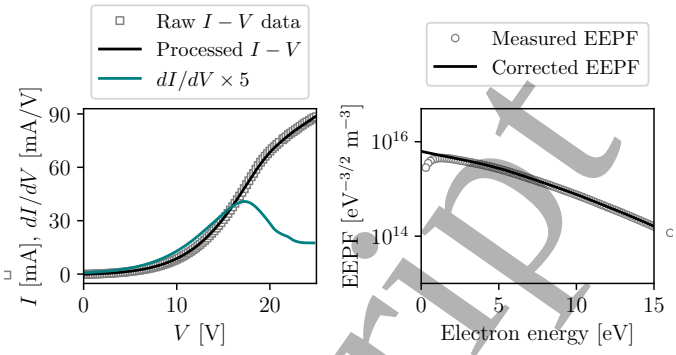

Fig. 3: Instance of experimental and processed I-V and EEPF curves. The procedures are discussed in Section "Method and diagnostics".

The experimental apparatus comprises nine electromagnets, six of which surround the discharge tube while three are placed around the expansion chamber. Only two coils are powered in this experiment. Following the nomenclature of [5], the first one, named GB2, is located at $z = 19$ cm and serves to generate the MN downstream the tube exit. The second one, named PB3, is located at $z = -25$ cm and it allows shaping the field topology inside the source. For the purpose of this analysis, two types of topologies are tested, as exemplified in Figure 1:

1. a simple magnetic nozzle as reference case, depicted in Figure 1(top). It is obtained setting $I_{GB2} = 9$ A and $I_{PB3} = 0$ A;

2. a specific configuration featuring a separatrix inside the source, see Figure 1(bottom). The same MN shape is preserved downstream the tube exit while the ECR condition is met near the antenna center. The coils currents are $I_{GB2} = 9$ A and $-5 < I_{PB3} < -1$ A.

A positive (negative) value of the coils current indicates that the relative B field points along the $+z$ ($-z$) direction. As the value of I_{PB3} is varied, the resonance region shifts along the tube axis. This is directly visible in Figure 2 which reports the axial profile of the magnetic field. In the general case of rf discharges when no resonance is required, an ECR region is present far upstream and far downstream, where a negligible amount of energy is deposited [6]. When PB3 is powered with a negative current, an additional resonance surface appears within the volume defined by the antenna, as desired. This simple reshaping of the field topology can conceivably underlie an enhancement of the electron properties.

It shall be remarked that, according to the generalized theory, typical helicon plasmas allow two wave modes to couple the antenna electromagnetic field, namely the he-

Accepted Manuscript

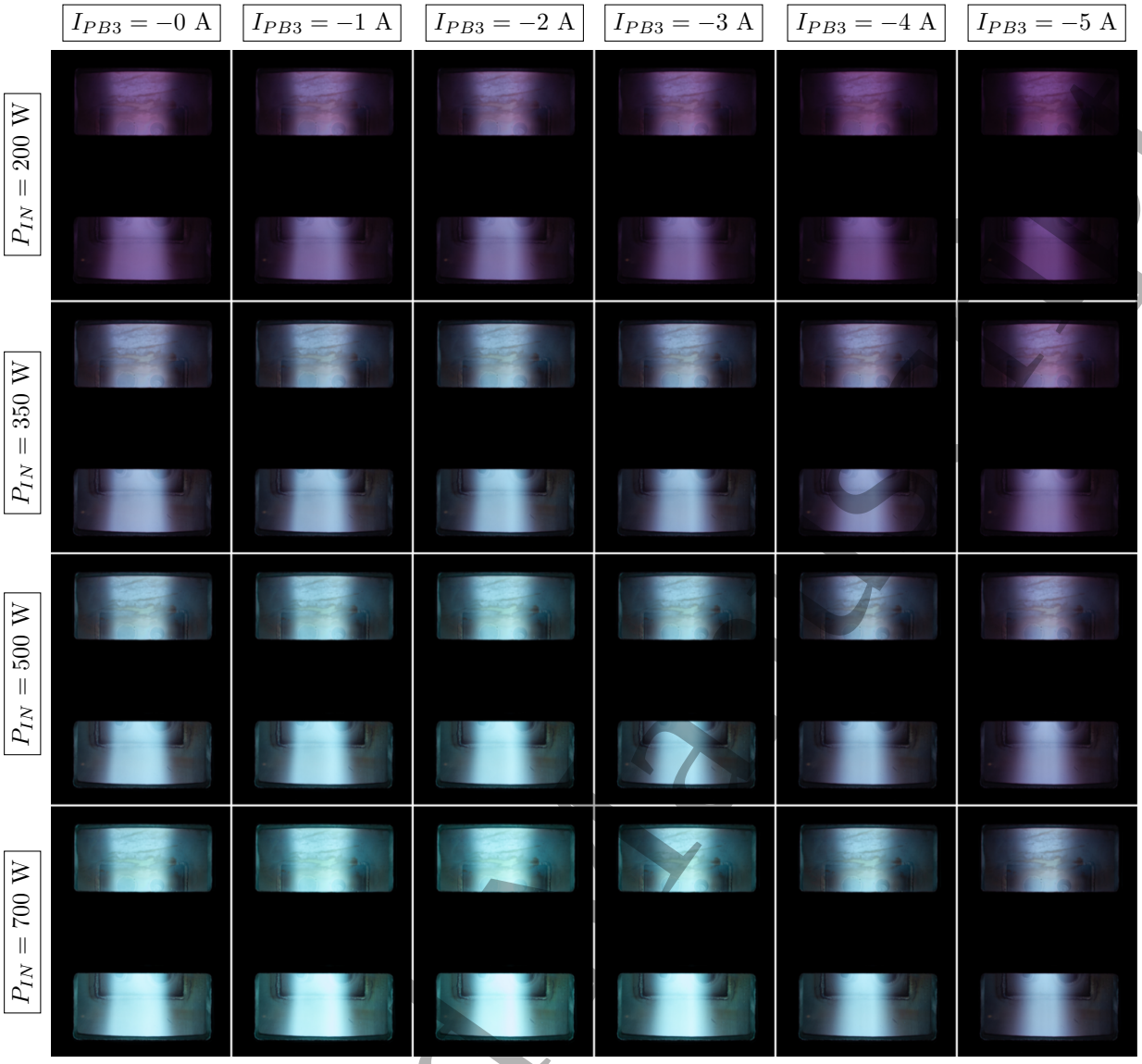

Fig. 4: Photographs (f/8, 1/30 s) of the plasma plume in the region $8 < z < 28$ cm. Rows and columns of the matrix are associated with a specific value of P_{IN} and I_{PB3}, respectively.

licon (H) and Trivelpiece–Gould (TG) modes [27]. However, when the external magnetic field is relatively weak, which is the case in this experiment to achieve ECR condition, only TG modes solve the dispersion relation. Hence, the discharge in analysis is most likely sustained in inductive mode with propagating TG waves, although H waves could in principle propagate downstream the antenna where magnetic field intensity and plasma density increase.

Method and diagnostics. – The experiment primarily consists in careful measurements of the electron energy probability function (EEPF) $f(\varepsilon)$ as the main external parameters are varied, namely input power P_{IN}, mass flow rate $\dot{m}$ and I_{PB3}. A rf-compensated Langmuir probe (RFCLP) is used, whose detailed description and characterization can be found in [5]. The tip is a tungsten wire with 0.38 mm diameter and 5 mm length. A series of chokes together with an auxiliary electrode ensure proper rf compensation [5]. In this experiment, the probe is oriented parallel to the magnetic field. I-V characteristics are recorded on-axis at $z = 0$ and $z = 31.5$ cm. Voltage sweep and current measuring are performed using a calibrated Keithley 2450 SourceMeter with about 15 Hz in step frequency. The EEPF is computed using the Druyvesteyn method [28, 29] and, accordingly, the electron density n_e and effective electron temperature T_{eff} are derived from the distribution function moments. Note that the magnetic field at the two probed locations is weak enough to guarantee an electron Larmor radius larger than the probe length, so that the classical Druyvesteyn theory applies [28]. The full probe characteristic, that is without subtraction of the ion current, is used for differentiation and

Accepted manuscript

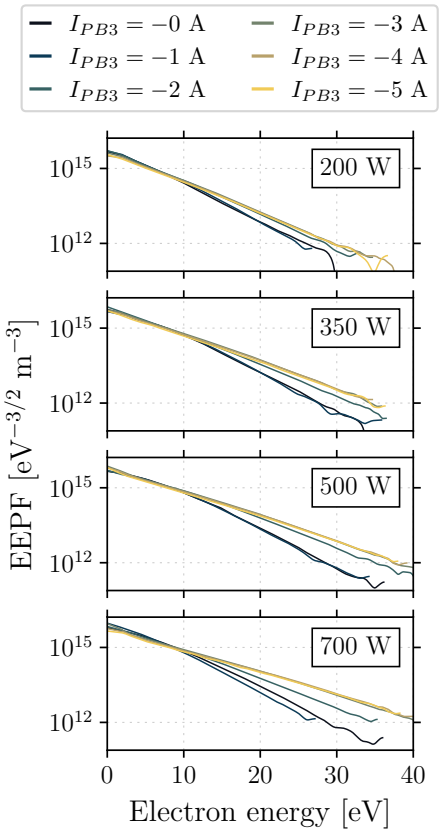

Fig. 5: EEPFs measured at $z = 0$ as function of P_{IN} and I_{PB3} with $\dot{m} = 0.2$ mg s^{-1} Xe.

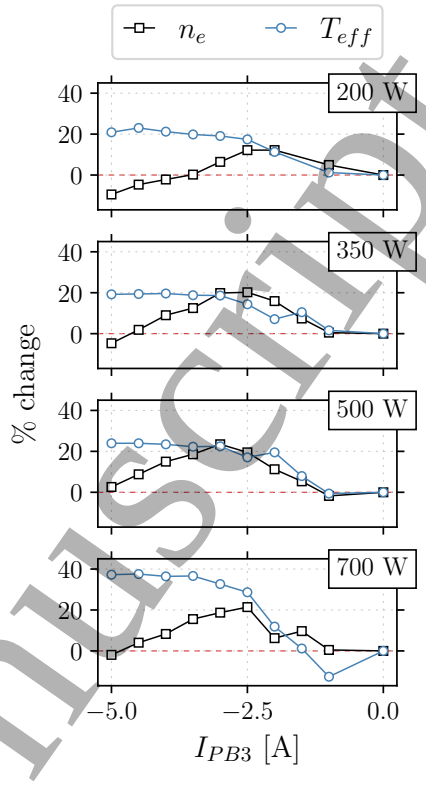

Fig. 7: Percentage change of n_e and T_e at $z = 0$ for different values of P_{IN} with $\dot{m} = 0.2$ mg s^{-1} Xe. Reference case: $I_{GB2} = 9$ A and $I_{PB3} = 0$ A.

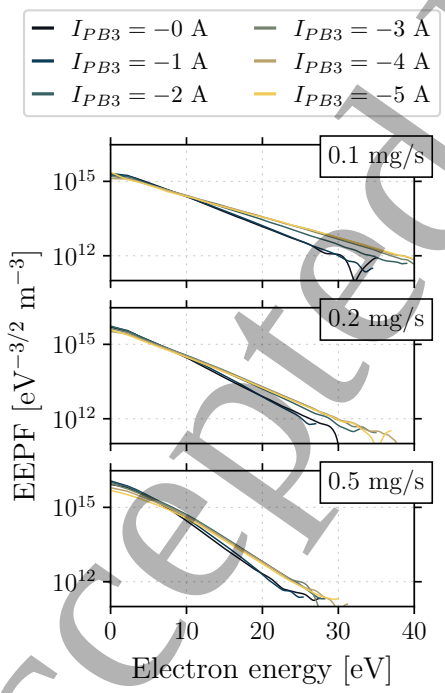

Fig. 6: EEPFs measured at $z = 0$ as function of $\dot{m}$ and I_{PB3} with $P_{IN} = 200$ W.

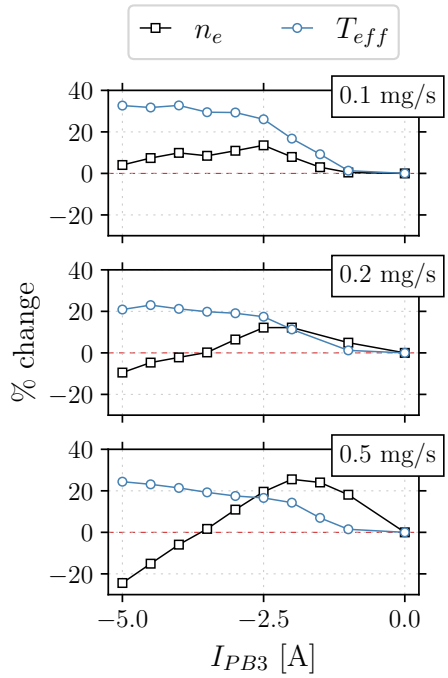

Fig. 8: Percentage change of n_e and T_e at $z = 0$ for different values of $\dot{m}$ with $P_{IN} = 200$ W. Reference case: $I_{GB2} = 9$ A and $I_{PB3} = 0$ A.

Accepted Manuscript

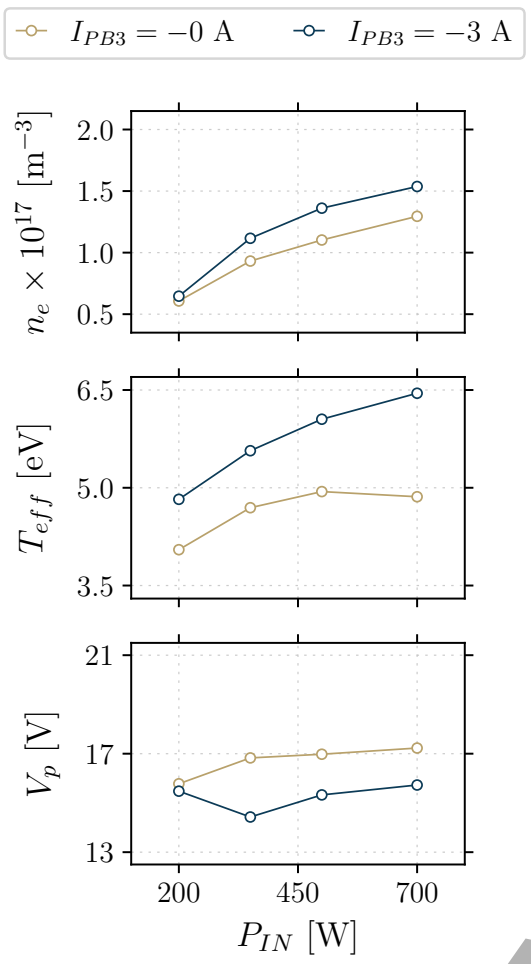

Fig. 9: Electron properties at $z = 0$ cm as a function of P_{IN} with $\dot{m} = 0.2$ mg s^{-1} Xe.

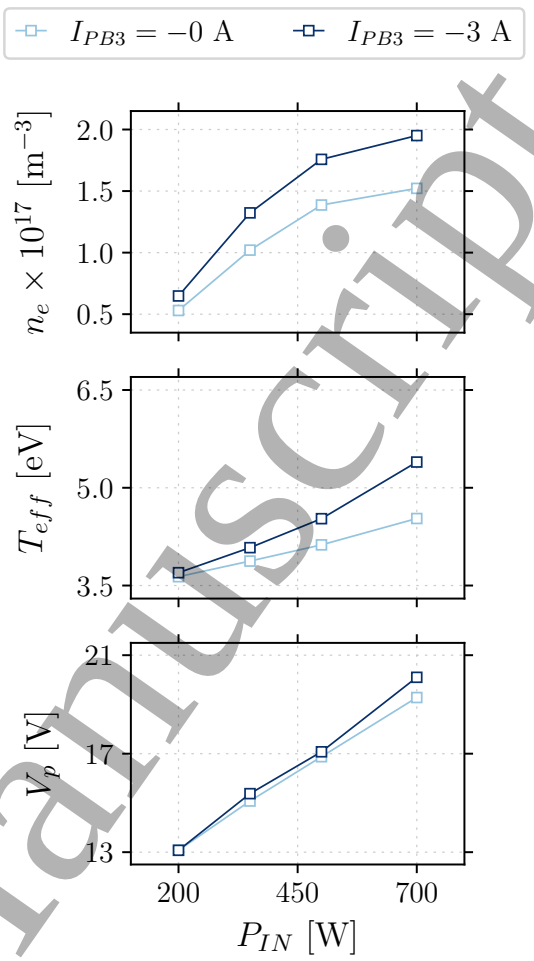

Fig. 10: Electron properties at $z = 31.5$ cm as a function of P_{IN} with $\dot{m} = 0.2$ mg s^{-1} Xe.

inference of the EEPF because of the issues discussed in [30]. Each I-V characteristic is interpolated and smoothed using local regression algorithms to minimize the noise coming from finite differentiation without introducing any artifact in the curve. Furthermore, the EEPFs retrieved in this work have been corrected at very low electron energies ($\varepsilon < 1 - 2$ eV). Experimental curves derived from double differentiation of the I-V characteristic always exhibit a depleted profile close to zero energy, whereas the EEPF theoretically increases up to $\varepsilon = 0$. Since the low energy electrons significantly contributes to the determination of n_e and T_{eff}, the correction procedure detailed in [30] has been applied herein. Figure 3 provides an example of raw data processing including I-V curve smoothing and interpolation as well as EEPF correction close to $\varepsilon = 0$.

Results and discussion. – Figure 4 is an array of photographs showing how the plasma beam appears when P_{IN} and I_{PB3} are varied. Regardless of the input power, the plasma plume becomes brighter around $I_{PB3} \simeq -2$ A. The color is also more greenish that certainly indicates a larger ionization degree and excitation of high-energy atomic optical transitions. This observation qualitatively indicates enhanced plasma properties when the ECR condition is met near the antenna.

Parametric EEPFs measured at $z = 0$ are shown in Figure 5 and Figure 6 as a function of input power and mass flow rate, respectively. To a large extend, electrons exhibit a clear Maxwellian behavior in all cases. One can observe that, as I_{PB3} is decreased in magnitude, electrons experience an effective heating. Indeed, the EEPF changes slope, favoring higher electron energies. This phenomenon is more pronounced at larger input powers and lower mass flow rates because the fraction of neutrals decreases and the collision frequency drops. By integrating the distribution function, n_e and T_{eff} are derived and shown in Figure 7 and Figure 8 in terms of percentage change with respect to the simple nozzle configuration. Absolute values, instead, are reported in Figure 9 for $I_{PB3} = 0$, -3 A, where the plasma potential V_p results from the first derivative of the electron current. The most significant result concerns the gain in T_{eff}. Values between 20 % up to nearly 40 % are measured as soon as $I_{PB3} < -2$ A. The

Accepted Manuscript

gain in T_{eff} flattens around $I_{PB3} = -3$ A, thus making a further reduction of I_{PB3} unnecessary. In addition, it is found that n_e grows by 20 % at $I_{PB3} \simeq -2$ A. When I_{PB3} is further decreased, the gain in n_e instead reduces, even reaching negative values in most cases. This phenomenon is linked to the axial location of the separatrix. At large negative currents driven in PB3, the magnetic separatrix moves downstream the antenna center. As a consequence, charged species are more likely transported towards $-z$, i.e. along the nozzle that forms upstream the antenna. This is qualitatively confirmed by a brighter plasma easily visible during experiments in the upstream part of the discharge tube. It becomes clear that a compromise between improved T_{eff} and greater plasma flux at the back plate shall be found to effectively enhance the overall performance. In this experimental configuration, a satisfactory gain in both n_e and T_{eff} is obtained at $I_{PB3} = -3$ A, regardless of the other external parameters.

Consequently, additional measurements are performed at $z = 31.5$ cm, that is in the divergent segment of the MN, at $I_{PB3} = 0$ A and $I_{PB3} = -3$ A. The probed plasma parameters are shown in Figure 10 as a function of P_{IN}. A remarkable gain in n_e and T_{eff} is also found downstream the MN throat. V_p raises as well, albeit less significantly with respect to the other quantities. As mentioned beforehand, the improvement is more significant at larger P_{IN}.

In the interpretation of the results reported above, one can clearly speculate on the role of parallel electron transport due to the different magnetic topologies. Given the cusp-like field in the source when the ECR condition is satisfied, hot electrons typically produced close to the antenna [31, 32] can be transported closer to the axis with respect to the customary MN configuration. Accordingly, the enhanced electron temperature measured along the discharge axis may partially result from such a transport phenomenon in addition to the resonant heating. Nevertheless, a larger electron energy in the central region of the plasma beam leads to a stepper radial gradient of electron pressure which consequently implies a larger magnetic thrust produced in the plume [9, 10, 33].

Conclusion. – In summary, effective electron heating is observed in the MN of a rf discharge at 13.56 MHz when the ECR condition is met near the antenna center by tuning the magnetic field topology. In such cases, measurements show that the electron temperature easily increases by 20 %, hitting 40 % at high power. This strategy could significantly contribute to improving the efficiency of rf propulsion systems which rely on MN acceleration especially at low and moderate power levels.

* * *

This project has received funding from the European Union's Horizon 2020 research and innovation program under grant agreement No 870542 (HelIcon PlasmA Thruster for In-space Applications).

Data availability. – The data that support the findings of this study are available upon reasonable request from the authors.

REFERENCES

[1] Bellomo N, Magarotto M, Manente M, Trezzolani F, Mantellato R, Cappellini L, Paulon D, Selmo A, Scalzi D, Minute M, Duzzi M, Barbato A, Schiavon A, Di Fede S, Souhair N, De Carlo P, Barato F, Milza F, Toson E and Pavarin D 2021 *CEAS Space Journal* ISSN 1868-2510 URL https://doi.org/10.1007/s12567-021-00374-4

[2] Moloney R, Karadag B, Fabris A L, Staab D, Frey A, Garbayo A, Shadbolt L, Azevedo E R, Faircloth D, Lawrie S and Tarvainen O 2019 *Experimental Validation and Performance Measurements of an ECR Thruster Operating on Multiple Propellants*

[3] Petro E M and Sedwick R J 2016 *Effects of Water Vapor Propellant on Helicon Thruster Performance* URL https://arc.aiaa.org/doi/abs/10.2514/6.2016-4735

[4] Shinohara S 2018 *Advances in Physics: X* **3** 185–220 ISSN 23746149 URL https://doi.org/10.1080/23746149.2017.1420424

[5] Vinci A E and Mazouffre S 2021 *Physics of Plasmas* **28** 033504 URL https://doi.org/10.1063/5.0037117

[6] Vinci A E and Mazouffre S 2021 *Journal of Applied Physics* **130** 183301 URL https://doi.org/10.1063/5.0069983

[7] Takahashi K 2021 *Scientific Reports* **11** 1–12 ISSN 20452322 URL https://doi.org/10.1038/s41598-021-82471-2

[8] Inchingolo M R, Merino M and Navarro-Cavallé J 2022 *37th International Electric Propulsion Conference, Massachusetts Institute of Technology, Cambridge, MA, USA, June 19-23, 2022*

[9] Ahedo E and Merino M 2010 *Physics of Plasmas* **17** 073501 URL https://doi.org/10.1063/1.3442736

[10] Takahashi K, Chiba A, Komuro A and Ando A 2016 *Plasma Sources Science and Technology* **25** 055011 URL https://doi.org/10.1088/0963-0252/25/5/055011

[11] Collard T A and Jorns B A 2019 *Plasma Sources Science and Technology* **28** 105019 URL https://doi.org/10.1088/1361-6595/ab2d7d

[12] Wachs B and Jorns B 2020 *Plasma Sources Science and Technology* **29** 045002 URL https://doi.org/10.1088/1361-6595/ab74b6

[13] Cannat F, Lafleur T, Jarrige J, Chabert P, Elias P and Packan D 2015 *Physics of Plasmas* **22** 053503 URL https://hal.archives-ouvertes.fr/hal-01229071

[14] Correyero S, Jarrige J, Packan D and Ahedo E 2019 *Plasma Sources Science and Technology* **28** 095004 URL https://doi.org/10.1088/1361-6595/ab38e1

[15] Nishiyama K, Hosoda S, Ueno K and Kunina H 2011 *32nd International Electric Propulsion Conference, Wiesbaden, Germany, September 11-15, 2011* URL http://electricrocket.org/IEPC/IEPC-2011-309.pdf

[16] Koizumi H, Komurasaki K, Aoyama J and Yamaguchi K 2014 *Transactions of the Japan Society for Aeronautical and Space Sciences, Aerospace Technology Japan* **12**

Accepted Manuscript

Tb_19–Tb_24 URL https://doi.org/10.2322/tastj.12.Tb_19

[17] Koizumi H, Kawahara H, Yaginuma K, Asakawa J, Nakagawa Y, Nakamura Y, Kojima S, Matsuguma T, Funase R, Nakatsuka J and Komurasaki K 2016 *Transactions of the Japan Society for Aeronautical and Space Sciences, Aerospace Technology Japan* **14** Pb_13–Pb_22 URL https://doi.org/10.2322/tastj.14.Pb_13

[18] Nishiyama K, Hosoda S, Ueno K, Tsukizaki R and Kuninaka H 2016 *Transactions of the Japan Society for Aeronautical and Space Sciences, Aerospace Technology Japan* **14** Pb_131–Pb_140 URL https://doi.org/10.2322/tastj.14.Pb_131

[19] Nakagawa Y, Koizumi H, Kawahara H and Komurasaki K 2019 *Acta Astronautica* **157** 294–299 ISSN 0094-5765 URL https://doi.org/10.1016/j.actaastro.2018.12.031

[20] Tani Y, Tsukizaki R, Koda D, Nishiyama K and Kuninaka H 2019 *Acta Astronautica* **157** 425–434 ISSN 0094-5765 URL https://doi.org/10.1016/j.actaastro.2018.12.023

[21] Packan D, Elias P, Jarrige J, Vialis T, Correyero S, Peterschmitt S, Porto-Hernandez J, Merino M, Sánchez-Villar A, Ahedo E, Peyresoubes G, Thorinius A, Denis S, Holste K, Klar P, Scharmann S, Zorn J, Bekemans M, Scalais T, Bourguignon E, Zurbach S, Azais P, Habbassi I, Mares M and Hoque A 2019 *36th International Electric Propulsion Conference, University of Vienna, Vienna, Austria, September 15-20, 2019* URL http://electricrocket.org/IEPC/IEPC_2017_547.pdf

[22] Chung C, Kim S S and Chang H Y 2002 *Phys. Rev. Lett.* **88**(9) 095002 URL https://link.aps.org/doi/10.1103/PhysRevLett.88.095002

[23] Chung C, Kim S S and Chang H Y 2004 *Phys. Rev. E* **69**(1) 016406 URL https://link.aps.org/doi/10.1103/PhysRevE.69.016406

[24] Vinci A E, Delaviè-Delion Q and Mazouffre S 2022 *Journal of Electric Propulsion* **1** URL https://doi.org/10.1007/s44205-022-00003-0

[25] Dietz P, Gärtner W, Koch Q, Köhler P E, Teng Y, Schreiner P R, Holste K and Klar P J 2019 *Plasma Sources Science and Technology* **28** 084001 URL https://doi.org/10.1088/1361-6595/ab2c6c

[26] Holste K, Dietz P, Scharmann S, Keil K, Henning T, Zschätzsch D, Reitemeyer M, Nauschütt B, Kiefer F, Kunze F, Zorn J, Heiliger C, Joshi N, Probst U, Thüringer R, Volkmar C, Packan D, Peterschmitt S, Brinkmann K T, Zaunick H G, Thoma M H, Kretschmer M, Leiter H J, Schippers S, Hannemann K and Klar P J 2020 *Review of Scientific Instruments* **91** 061101 URL https://doi.org/10.1063/5.0010134

[27] Chen F and Arnush D 1997 *Physics of Plasmas* **4** 3411–3421 URL https://doi.org/10.1063/1.872483

[28] Godyak V A and Demidov V I 2011 *Journal of Physics D: Applied Physics* **44** 233001 URL https://doi.org/10.1088/0022-3727/44/23/233001

[29] Lobbia R B and Beal B E 2017 *Journal of Propulsion and Power* **33** 566–581 URL https://doi.org/10.2514/1.B35531

[30] Godyak V 2021 *Journal of Applied Physics* **129** 041101 URL https://doi.org/10.1063/5.0024258

[31] Takahashi K, Charles C, Boswell R, Cox W and Hatakeyama R 2009 *Applied Physics Letters* **94** 191503 URL https://doi.org/10.1063/1.3136721

[32] Takahashi K, Akahoshi H, Charles C, Boswell R W and Ando A 2017 *Physics of Plasmas* **24** 084503 URL https://doi.org/10.1063/1.4990110

[33] Takahashi K, Lafleur T, Charles C, Alexander P and Boswell R W 2012 *Physics of Plasmas* **19** 083509 URL https://doi.org/10.1063/1.4747701

Accepted Manuscript